Available online at www.sciencedirect.com
ScienceDirect
Journal of Power Sources 178 (2008) 547–553
JOURNAL OF POWER SOURCES
www.elsevier.com/locate/jpowsour

High utilization of Pt nanocatalysts fabricated using a high-pressure sputtering technique

Sung Jong Yoo [a], Yong-Hun Cho [a], Hyun-Seo Park [a], Joong Kee Lee [b], Yung-Eun Sung [a,*]

[a] *School of Chemical and Biological Engineering & Research Center for Energy Conversion and Storage, Seoul National University, Seoul 151-744, Republic of Korea*
[b] *Advanced Energy Materials Processing Laboratory, Korea Institute of Science & Technology, Seoul 130-650, Republic of Korea*

Received 14 July 2007; received in revised form 18 September 2007; accepted 24 September 2007
Available online 5 October 2007

Abstract

Pt nanocatalysts formed on a gas diffusion layer substrate for use in proton exchange membrane fuel cells were fabricated by using a high-pressure sputtering technique in a gaseous mixture of Ar and He. Rather than the dense film deposited by conventional sputtering techniques, the resulting structure was comprised of a porous Pt nanocatalyst layer with an average particle size of 8.9 nm. The porous Pt nanocatalysts were characterized by scanning electron microscopy, transmission electron microscopy, X-ray diffraction, and X-ray absorption near edge spectroscopy. Compared with the dense Pt catalyst layer, the electrochemical activated surface of the porous Pt nanocatalyst layer, measured using cyclic voltammetry, was enhanced about 250%. Polarization characteristics of the membrane electrode assembly, which utilized the porous Pt nanocatalyst layer in the proton exchange membrane fuel cells, showed that the maximum power density per unit area increased with an increase in the sputtering pressure. The high performance of Pt nanocatalysts fabricated at a sputtering pressure of 200 mTorr (Ar/He = 1) was due to miniaturization of the Pt particles and formation of the porous catalyst layer.

Keywords: Pt nanocatalysts; Sputtering technique; Proton exchange membrane fuel cells (PEMFCs); Utilization of Pt

1. Introduction

Polymer electrolyte membrane fuel cells (PEMFCs), which directly convert chemical energy into electrical energy, are promising and worthy candidates for high efficiency and low emission energy conversion devices in mobile, stationary and portable application sectors [1–3]. However, there are major barriers to the commercialization of such applications, as follows: the high cost of the electrocatalyst (Pt) and the solid polymer electrolyte (Nafion), and the high electrocatalyst loading (>0.4 mg Pt cm^{-2}) required [4,5]. One important goal when applying PEMFCs technology is to reduce the amount of electrocatalyst required without sacrificing performance. Therefore, the utilization of Pt catalysts plays an important role in practical application of PEMFCs.

In recent years, several articles devoted to the study of minimizing Pt loading have been published. One approach is to use carbon-supported noble metal catalysts with a high surface area to enhance catalytic performance and utilization efficiency [6,7]. Remarkable progress was made by Wilson and Goffesfeld who prepared the catalyst layer by mixing the soluble inomer with the Pt/C catalysts and applied the mixture to the electrolyte membrane. As a result of these studies, a performance of about 0.6 V at 1 A cm^{-2} was obtained with a Pt loading of 0.13 mg cm^{-2} in H_2/air operation, 3/5 atm of pressure, and 105/90 °C ($T_{cell}/T_{humidifiers}$) with membrane Nafion 117 (from Fig. 4 of Ref. [6]). Recently, however, carbon corrosion has been recognized as problem during long-term operation or cell reversal in the case of reactant storage. Nevertheless, Pt utilization in the Pt/C catalysts was still lower (20%) [8,9], because the soluble inomer cannot penetrate the carbon pore (primary pore diameter < 100 nm), on which most of the Pt (>85%) is located [10]. Another approach is to form catalyst layers by using direct sputter deposition. Srinivasan et al. deposited a Pt layer on the gas diffusion layer (GDL) using a sputtering

* Corresponding author. Tel.: +82 2 880 1889; fax: +82 2 888 1604.
E-mail address: ysung@snu.ac.kr (Y.-E. Sung).

0378-7753/$ – see front matter © 2007 Elsevier B.V. All rights reserved.
doi:10.1016/j.jpowsour.2007.09.098

technique. In this system, cell performance at a loading of 0.45 mg Pt cm^{-2} was equivalent to that of conventional methods at a loading of 4.0 mg Pt cm^{-2} [11]. Hirano et al. deposited a Pt layer (0.1 mg cm^{-2}), as a cathode electrode, using a sputter technique on an uncatalyzed GDL. This modification resulted in enhanced cell performance [12]. O'Hayre et al. compared the power density of a commercial membrane electrode assembly (MEA) loaded with 0.4 mg Pt cm^{-2} to that of a MEA with 0.04 mg Pt cm^{-2} (15 nm) fabricated using the sputtering technique. The results showed that 3/5 of the maximum power density was produced with 1/10 the catalyst loading [13]. However, conventional sputtered Pt catalyst layers suffered from the deposition of Pt as a conformal film on the substrate [14]. Due to this compact and dense structure, the Pt catalyst layer was not porous, and displayed a small electrochemical active surface (EAS) area.

Recently, it has been reported that a high-pressure (>100 mTorr) sputtering technique can produce nanoscale particles, which form in the vapor as a result of the high pressure [15,16]. The sputtered atoms undergo many collisions in the vapor at these high pressures, subsequently nucleate, and grow in the vapor by rapid condensation. It is expected that the Pt catalyst layer formed using the high-pressure sputtering technique leads to an improvement in the Pt microstructure, such that the Pt catalysts layer is more porous, allowing enhanced Pt utilization.

This study investigated Pt nanocatalysts deposited using a high-pressure radio frequency (RF) magnetron sputtering technique with a mixture of gaseous Ar and He for use in PEMFCs. Nanoscale Pt particles were achieved using a sputtering pressure (200 mTorr, Ar/He = 1) that was higher than that used in normal thin film processing (1–10 mTorr, Ar/He = 1). Pt nanocatalysts processed using this method were characterized by scanning electron microscopy (SEM), transmission electron microscopy (TEM), atomic force microscopy (AFM), X-ray absorption near edge spectroscopy (XANES), and X-ray diffraction (XRD). Cyclic voltammetric measurements (CV), electrochemical polarization curves and single cell performance of MEA utilizing the synthesized Pt nanocatalyst layers were analyzed.

2. Experimental

2.1. Fabrication of Pt nanocatalysts using the sputter technique

The Pt nanocatalysts deposited on a gas diffusion layer were fabricated using a RF magnetron sputter technique at high pressure. Pt (Pt 99.99%, United Vacuum & Materials) was used as the target material. The base pressure was less than 1×10^{-6} Torr and the working pressure was controlled variously from 11 to 200 mTorr. The working distance between the sputter target and substrate was 23 cm. Sputtering was carried out under an atmosphere of Ar and He (volume ratio of 1:1) at room temperature. The amount of sputtered Pt catalyst produced was calculated from the weight change in the amount of loaded Pt; the amount of Pt nanocatalyst could be controlled by sputtering working pressure, time, and RF power.

2.2. Structure characterizations

Structural analyses were carried out using TEM, TED, XANES, XRD, AFM, and SEM. TEM images were obtained using a JEOL EM-2000 EX II microscope at an accelerating voltage of 200 kV. Cu grids were used as the substrate and for TEM analysis. XRD (MAC Science M18XHF-SRA equipped with a Cu Kα source at 30 kV–30 mA) analyses of as-prepared electrodes were used to determine the degree of crystallinity. The morphology of all samples was carefully measured by planar-sectional SEM (JEOL 6330F) and AFM (SPA-400, Seiko instrument). Pt L_{III} edge XANES were recorded using the 7C beam line at the Pohang Light Source (PLS) with a ring current of 120–170 mA at 2.5 GeV. A Si (1 1 1) monochromator crystal was used after detuning the intensity to 85% to eliminate high-order harmonics. The data were collected in fluorescence and transmission modes. Energy calibrations were carried out for all measurements by placing Pt foil in front of the third ion chamber and assigning the first inflection point to 11564 eV.

2.3. Electrochemical and fuel cell testing

Performance of PEMFC that used the sputtered Pt nanocatalysts was evaluated by measuring cell voltage of a 5-cm^2 cross-section of the catalyst zone under constant current conditions with a potentiometer. The commercial catalyst ink was prepared from a mixture of Pt/C (40 wt.%, Johnson Matthey (JM)) powder, isopropyl alcohol, Nafion solution (5 wt.%, Dupont) and deionized water. The cathode and anode consisted of sputtered Pt nanocatalysts at a loading of 0.02 mg cm^{-2}, respectively, i.e. total loadings of 0.04 mg cm^{-2} per MEA. To compare the high-pressure sputtering and conventional ink methods, JM catalysts were used at a loading of 0.3 mg cm^{-2} anode and 0.3 mg cm^{-2} cathode, i.e. total loadings of 0.6 mg cm^{-2} per MEA. To evaluate EAS, CV was carried out with flowing deionized water at the anode, as the working electrode, and flowing hydrogen at the cathode, as the counter-electrode and as the dynamic hydrogen electrode (DHE), at a scan rate of 50 mV s^{-1}.

The current–voltage characteristics of each MEA sample were measured in a 5-cm^2 single cell (CNL-PEM005-01, CNL Energy). The single cell consisted of two graphite plates with serpentine flow-fields and two metal end-plates adjacent to the graphite plates. The MEA fabricated in this study was formed using Nafion 112 as the polymer electrolyte membrane. Before use, Nafion 112 was pretreated in a hydrogen peroxide solution (3 wt.%) for about 1 h at 100 °C followed by washing in deionized water for 1 h. The procedure described above was repeated, and the membrane then was boiled in a sulfuric acid solution (0.5 M) for 1 h and washed in boiling deionized water for 1 h. The prepared GDL and MEA were placed between two graphite plates, which then were assembled using the appropriate pressure. For the performance measurements, a humidified hydrogen and oxygen, at stoichiometric ratio of 1.5:2, was fed to the anode and cathode side of the single cell at a temperature of 75/70 °C. During the measurement, the temperature was maintained at 70 °C and the pressure was held constant at atmospheric

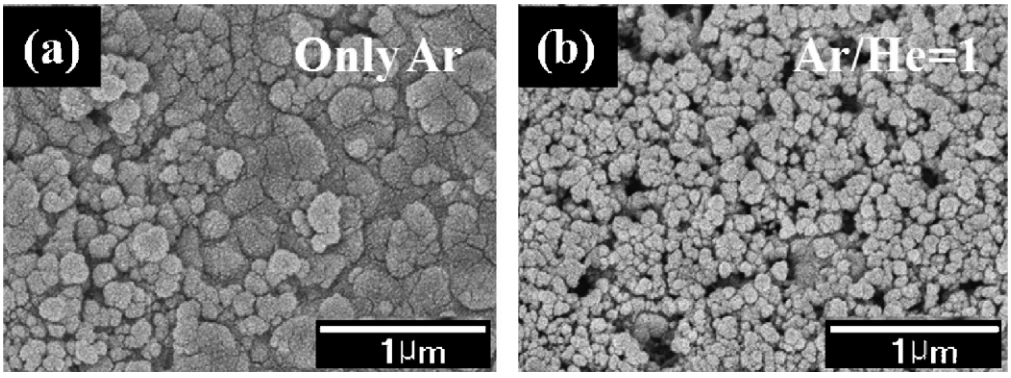

Fig. 1. SEM images of Pt catalyst layers deposited on the GDL substrate using sputtering technique with (a) only Ar (11 mTorr) and (b) both Ar and He (5.5 mTorr of Ar, total pressure 11 mTorr).

pressure. The cell voltage of each sample was obtained with increasing current density using a fuel cell test station (FCTS, Won-a tech) to measure the current–voltage curves [17].

3. Results and discussion

Fig. 1(a) shows a typical SEM image of a dense Pt thin film produced on the GDL substrate by sputtering at 11 mTorr pressure with Ar (no He) gas. This image indicates that condensation of Pt particles induced by Ar gas results in the formation of a dense thin film. Fig. 1(b) presents a SEM image of Pt nanoparticles on the GDL substrate that resulted when He (5.5 mTorr) gas was added to the Ar (5.5 mTorr) gas. The average Pt nanoparticles diameter was about 95 nm and the size distribution was broad. As is evident in Fig. 1, Ar and He gas pressure critically affect Pt nanoparticle production. Recent papers have reported that Ar gas is responsible for the sputtering process, while Pt particle condensation is effectively induced by He gas [19]. That is, the sputtering process induced by Ar gas creates the Pt atomic species, which, in turn, form Pt nanoparticles upon induction by He gas.

Fig. 2 shows SEM images of the variation in Pt nanoparticle size induced by the different sputtering pressures (Ar/He = 1) on the Si (1 0 0) substrates. Pt nanoparticle size increased at lower sputtering pressures, indicating the growth of nanoparticle nucleation. Fig. 2(a) shows the formation of a dense film formation, which indicates that sputtering occurred below the supersaturated vapor pressure. Fig. 2(d) shows the result of

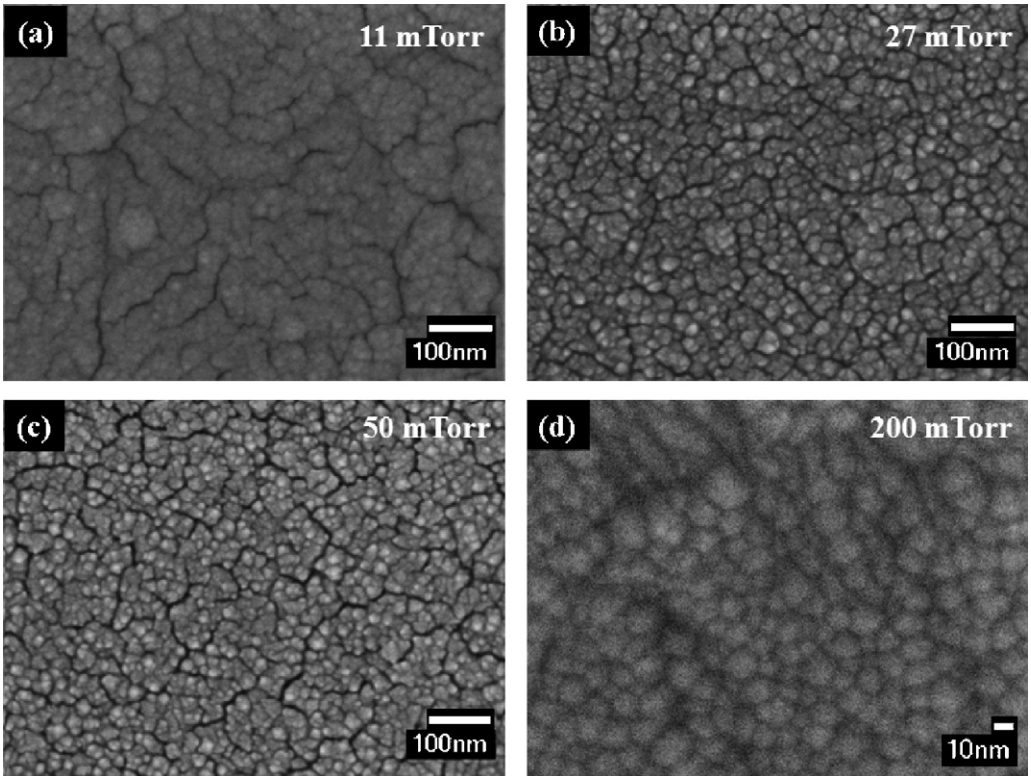

Fig. 2. SEM images of Pt catalyst layers deposited on the Si (1 0 0) substrate using different sputtering pressures with a mixture of gaseous Ar and He (Ar/He = 1). (a) 11 mTorr, (b) 27 mTorr, (c) 50 mTorr, and (d) 200 mTorr.

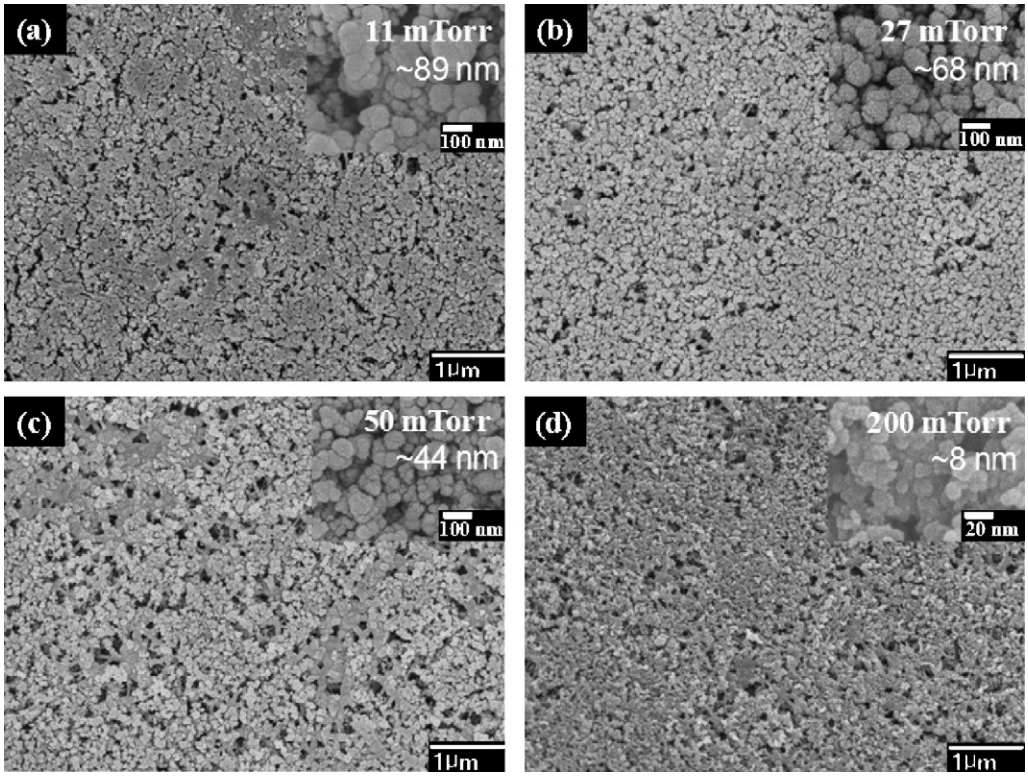

Fig. 3. SEM images of Pt catalyst layers deposited on the GDL substrate using different sputtering pressures with a mixture of gaseous Ar and He mixture (Ar/He = 1). (a) 11 mTorr, (b) 27 mTorr, (c) 50 mTorr, and (d) 200 mTorr. The inset represents the high magnification images.

depositing Pt nanoparticles at a pressure of 200 mTorr, i.e., above the supersaturated vapor pressure. The narrowness of the distribution is consistent with an average Pt nanoparticle size of 9.8 ± 2 nm. This result indicates that the Ar and He gas pressures determine the size range of the Pt particles produced by sputtering and subsequent condensation. Therefore, careful optimization of the gas pressure provides the versatility to produce, from a source of Pt atoms, a range of particle sizes, from a few atoms to a few thousand of atoms per nanoparticle, depending on the sputtering pressure. In general, it has been reported that the growth of nanoparticles occurs in two stages [18,19]. Energetic atoms sputtered from the target are cooled by He gas, leading to the nucleation of nanoscale particles. For the nucleation of Pt atoms, a three-body collision between two sputtered atoms and a cooling He atom is essential, as it removes excess kinetic energy from the sputtered atoms. The growth of particles also occurs via two-body collisions, such as cluster–cluster collisions [20]. The two- and three-body collisions occur more frequently at high supersaturated vapor pressure compared with normal gas pressures. Therefore, well-defined nanoscale structures can be fabricated by controlling the sputtering pressure.

SEM images of Pt deposited on GDL substrate using different sputtering pressures are shown in Fig. 3. Fig. 3(a) shows the dense Pt thin-film layer produced at 11 mTorr pressure. At 200 mTorr pressure, only Pt nanoparticle formation, but not film formation, was observed. The average size of the Pt nanoparticles decreased with increasing pressure and the size distribution narrowed.

The size of Pt nanoparticles on the GDL substrate produced at 200 mTorr pressure was confirmed by the XRD patterns shown in Fig. 4(a) and the average size of the Pt particles was about 8 nm, as calculated using the Debye–Scherrer equation [21]. The size of the Pt nanoparticles also was determined by means of the TEM images shown in Fig. 4(b). The dark points correspond to the Pt nanoparticles (~8.5 nm) and the crystalline plane of the Pt nanophase representing the *d*-spacing of the (1 1 1) plane ($d_{1\,1\,1} \sim 0.227$ nm) can be observed; this result was in agreement with the value for crystalline Pt. The formation of polycrystalline Pt also was confirmed by TED analysis of the (1 1 1), (2 0 0), (2 2 0), (3 1 1), and (2 2 2). The presence of well-defined Pt nanoparticles also was confirmed by the AFM image shown in Fig. 4(d).

Fig. 5 illustrates the size distribution of the Pt nanoparticles as a function of the sputtering pressure. One hundred particles were measured to study the size distribution of the Pt nanoparticles. The SEM images (Fig. 3) showed that the diameters of Pt nanoparticles varied from ~89 to ~8 nm as the sputtering pressure decreased. The kinetic energy with which the atoms and particles arrive at the GDL substrate determines the size of the resulting nanoparticles. The kinetic energy of the particles depends on the sputtering conditions.

XANES can give detailed information on the electronic states of the element under investigation. The normalized Pt L_{III} edge XANES spectra for the Pt nanoparticles on the GDL substrate are shown in Fig. 6. The peak appearing at the L_{III} X-ray absorption edge is called the "white line." It is considered to be due to the electronic transition from a core level ($2p_{3/2}$ for the L_{III}

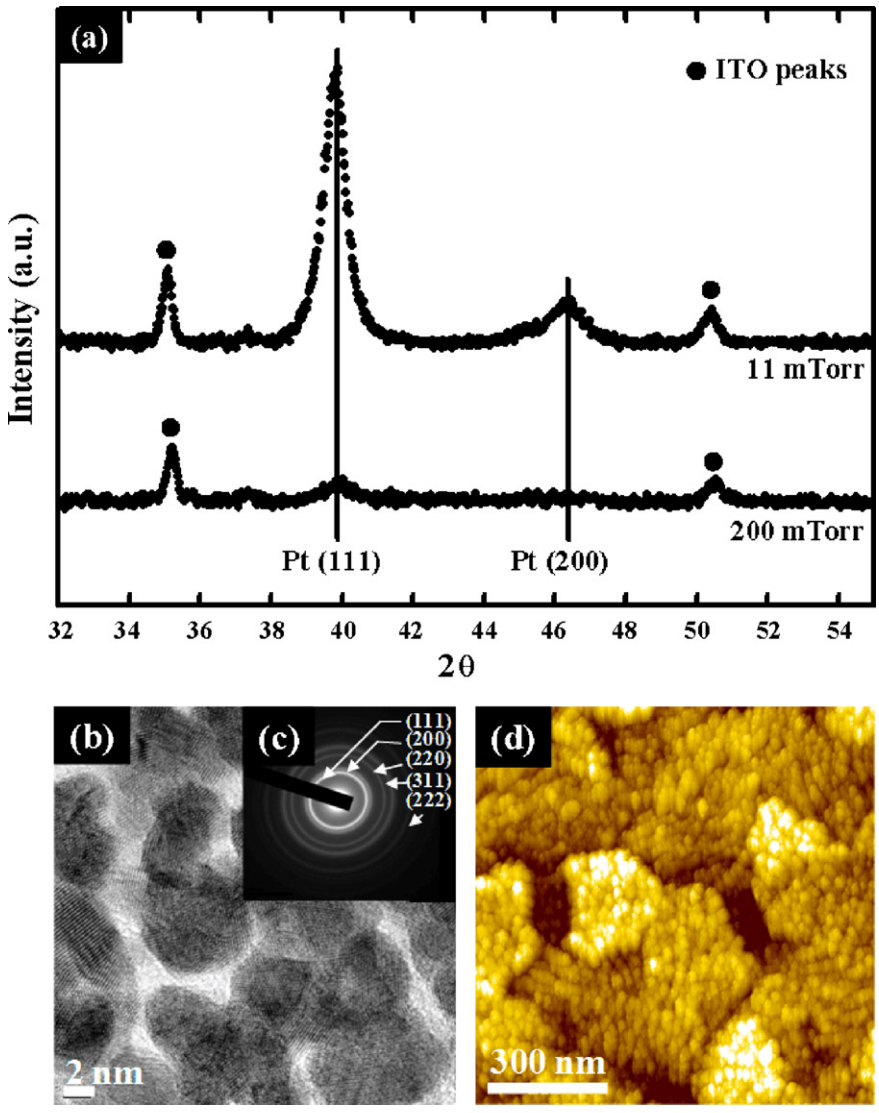

Fig. 4. (a) XRD pattern for different sputtering pressures, (b) high-resolution TEM image, (c) TED pattern, and (d) AFM image of Pt nanocatalysts deposited at a sputtering pressure of 200 mTorr (Ar/He = 1).

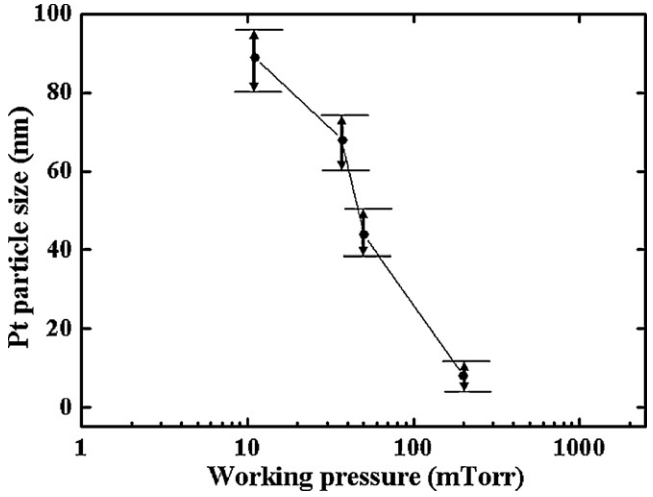

Fig. 5. Average particle sizes of Pt nanocatalysts as a function of the sputtering pressure with a mixture of gaseous Ar and He (Ar/He = 1).

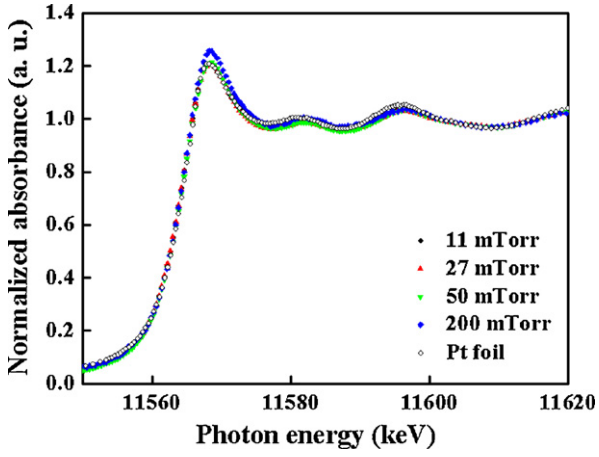

Fig. 6. Normalized Pt L_{III} edge XANES spectra of reference Pt foil (◯) and Pt nanocatalysts formed at different sputtering pressures of 11 mTorr (●), 27 mTorr (▲), 50 mTorr (▼), and 200 mTorr (◆) with a mixture of gaseous Ar and He mixture (Ar/He = 1).

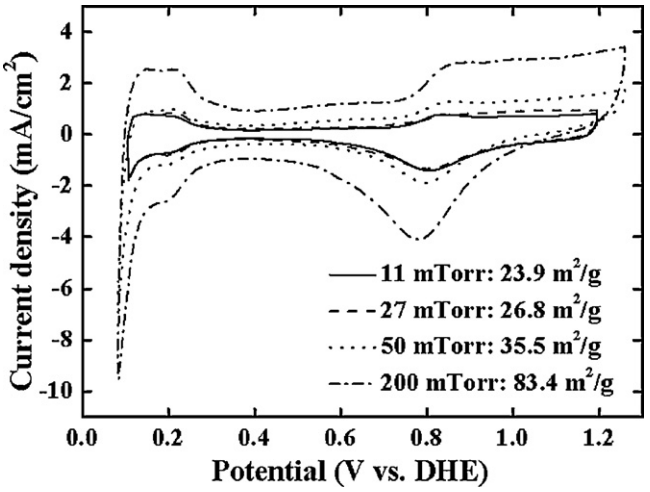

Fig. 7. Voltammetric plots of Pt nanocatalysts formed at different sputtering pressures of 11, 27, 50, and 200 mTorr with a mixture of gaseous Ar and He mixture (Ar/He = 1) under conditions of deionized water flowing at the anode and humidified hydrogen flowing at the cathode with a scan rate of 50 mV s^{-1} at room temperature.

edge) to vacant d-states of the absorbing atom. Accordingly, the white line is used to evaluate the density of the 5d-band vacancy. Fig. 6 shows that as Pt particle size increased, the d-band vacancy decreased. This result suggests that as particle size increases, the d-electron number of the 5d-band state with empty states above the Fermi level is reduced. These studies demonstrate that d-band vacancy depends on Pt particle size [22,23]. This provides additional evidence for the particle size effect.

Based on these results, it was concluded that particle size is a function of sputtering pressure. At very low pressures, the motion of the sputtered atoms is essentially that of an elastic collision, and a continuous film is formed on the GDL substrate. At higher gas pressures, the sputtered atoms undergo collision-induced aggregation. Therefore, not only do the atoms sputtered at high pressure arrive at the GDL substrate in the form of nanoscale particles, they also arrive with lower kinetic energies. A nanoscale particle is thereby promoted, particularly if energetic atoms sputtered from the target are cooled by the He gas.

CV was employed to obtain the EAS of Pt nanocatalysts deposited at different sputtering pressures. Fig. 7 shows the CV obtained with flowing deionized water at the anode, as the working electrode, and flowing of hydrogen at the cathode, as the counter-electrode as well as the DHE. The EAS ($m^2\ g^{-1}$) of Pt nanocatalysts was calculated using the columbic charge for hydrogen desorption ($Q_{Pt\text{-}H}$: assuming 210 μC cm^{-2} (Pt-H) of polycrystalline platinum) during the electro-adsorption and desorption of H_2 on Pt sites. The contribution of double layer charge was evaluated for every sample. The area obtained from the hydrogen desorption region can be correlated to the active surface area by the following equation [24]:

$$\mathrm{EAS} = \frac{Q}{L Q_{\mathrm{Pt\text{-}H}}} \quad (1)$$

where L is catalyst loading in the electrode.

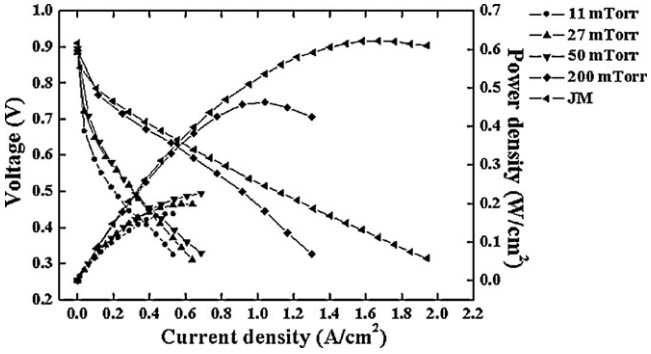

Fig. 8. Polarization curves and power density curves of MEAs with JM catalyst (◄) and Pt nanocatalyst layers formed at different sputtering pressures of 11 mTorr (●), 27 mTorr (▲), 50 mTorr (▼), and 200 mTorr (♦) with a mixture of gaseous Ar and He mixture (Ar/He = 1).

The EAS area data showed the contrast between the dense Pt catalyst layer obtained by the conventional sputtering process (low sputtering pressure) and the porous Pt nanocatalysts layer obtained by the high-pressure sputtering process. As shown in Fig. 7, the EAS of the porous Pt nanocatalyst layer (200 mTorr) was enhanced 250% enhancement compared with the dense Pt catalyst (11 mTorr). This result shows that the porous Pt nanocatalyst layer obtained by the high-pressure sputtering process has increased electrochemical reaction sites due to enhanced utilization of the Pt nanocatalysts.

Fig. 8 compares the electrochemical performances of PEMFC single cells made using Pt nanocatalysts formed at four different sputtering pressures: 11, 27, 50, and 200 mTorr. In all cases, equivalent amounts of Pt (0.02 mg cm^{-2}) were added to the anode and cathode. Fuel cell performance curves were measured after allowing for a steady reading at each point during the current scan, as controlled by the fuel cell test station. The open circuit voltage of all samples sputtered at 11–200 mTorr pressure showed an open circuit voltage of ~0.9 V, which is close to that of commercial Pt catalysts. From Fig. 8, the results of the fuel cell performance of the Pt catalyst layers sputtered at 11, 27, and 50 mTorr show that the maximum power density per unit area increased slightly with an increase in the sputtering pressure. In particular, the fuel cell performance of Pt nanocatalysts (total loadings of 0.04 mg cm^{-2} per MEA) sputtered at 200 mTorr pressure showed a maximum power density of 420 mW cm^{-2}, which was comparable to the 610 mW cm^{-2} for the JM catalyst (40 wt.% Pt/C, total loadings of 0.6 mg cm^{-2} per MEA). However, the efficiency per total weight (10.5 W mg^{-1}) of the sputtered Pt nanocatalysts was 10-fold greater than that of the JM catalyst (1 W mg^{-1}). This finding indicates that the Pt nanocatalyst layer electrode fabricated using a high-pressure sputtering technique in a mixture of gaseous Ar and He gas has an improved electrochemical surface reaction efficiency and utility even with low catalyst loading.

4. Conclusions

Pt nanocatalysts, for use in PEMFCs, were fabricated by using a RF magnetron sputtering technique at high pressure with a mixture of gaseous Ar and He mixture gas. The size range of

the Pt particles produced by the sputtering and condensation process was determined by the Ar and He pressures. The Pt nanocatalyst layer sputtered at 200 mTorr pressure consisted of nanoparticles with an average size of 8.9 nm. The electrochemical activated surface, measured using cyclic voltammetry, of the porous Pt nanocatalyst layer was enhanced 250% compared with the dense Pt catalyst layer. The fuel cell performance of Pt nanocatalysts formed using high-pressure sputtering deposition showed a maximum power density of 420 mW cm^{-2} and efficiency per total weight of 10.5 W mg^{-1}, which were comparable to the performance characteristics of a commercial catalyst.

Acknowledgments

This work was financially supported by Korea Research Foundation (Grant #KRF-2004-005-D00064), KOSEF through the Research Center for Energy Conversion and Storage, and National RD&D Organization for Hydrogen & Fuel Cell & Ministry of Commerce, Industry and Energy. We are grateful to Pohang Light Source (PLS) for allowing us to conduct our XAS measurements at their facility.

References

[1] T.E. Springer, T.A. Zawodzinski, S. Gottesfeld, J. Electrochem. Soc. 138 (1991) 2334.
[2] C.K. Dyer, J. Power Sources 106 (2002) 31.
[3] K.-W. Park, Y.-E. Sung, J. Ind. Eng. Chem. 12 (2006) 165.
[4] S. Litster, G. McLean, J. Power Sources 130 (2004) 61.
[5] G.J.K. Acres, J.C. Frost, G.A. Hards, R.J. Potter, T.R. Ralph, D. Thompsett, G.T. Burstein, G.J. Hutchings, Catal. Today 38 (1997) 393.
[6] M.S. Wilson, S. Goffesfeld, J. Electrochem. Soc. 139 (1992) L28.
[7] Y.G. Chun, C.S. Kim, D.H. Peck, D.R. Shin, J. Power Sources 71 (1998) 174.
[8] O.J. Murphy, G.D. Hitchens, D.J. Manko, J. Power Sources 47 (1994) 353.
[9] X. Cheng, B. Yi, M. Han, J. Zhang, Y. Qiao, J. Yu, J. Power Sources 79 (1999) 75.
[10] M. Watanabe, K. Makita, H. Usami, S. Motoo, J. Electroanal. Chem. 195 (1985) 81.
[11] S. Srinivasan, D.J. Manko, H. Koch, M.A. Enayetullah, A.J. Appleby, J. Power Sources 29 (1990) 367.
[12] S. Hirano, J. Kim, S. Srinivasan, Electrochim. Acta 42 (1997) 1587.
[13] R. O'Hayre, S.-J. Lee, S.-W. Cha, F.B. Prinz, J. Power Sources 109 (2002) 483.
[14] C.A. Cavalca, J.H. Arps, M. Murthy, US Patent no. 6,300,000 (2001).
[15] H. Hahn, R.S. Averback, J. Appl. Phys. 67 (1990) 1113.
[16] G.M. Chow, R.L. Holtz, A. Pattnaik, A.S. Edelstein, T.E. Schlesinger, R.C. Cammarata, Appl. Phys. Lett. 56 (1990) 1853.
[17] K.-W. Park, B.-K. Kwon, J.-H. Choi, I.-S. Park, Y.-M. Kim, Y.-E. Sung, J. Power Sources 109 (2002) 440.
[18] S. Yatsuya, T. Kamakura, K. Yamauchi, K. Mihama, Jpn. J. Appl. Phys. 25 (1986) 42.
[19] C.G. Granqvist, R.A. Buhrman, J. Appl. Phys. 47 (1976) 2200.
[20] J.M. Soler, N. Garcia, Phys. Rev. Lett. 49 (1982) 1857.
[21] V. Radmilvic, H.A. Gasteiger, P.N. Ross, J. Catal. 154 (1995) 98.
[22] D.R. Short, A.N. Mansour Jr., J.W. Cook, D.E. Sayers, J.R. Katzer, J. Catal. 82 (1983) 299.
[23] H. Yoshitake, Y. Iwasawa, J. Phys. Chem. 95 (1991) 7368.
[24] Z. Hou, B. Yi, H. Zhang, Electrochem. Solid-State Lett. 6 (2003) 232.